J|A|C|S
ARTICLES
Published on Web 09/25/2004

Extensive Migration of Ni and Mn by Lithiation of Ordered $LiMg_{0.1}Ni_{0.4}Mn_{1.5}O_4$ Spinel

Marnix Wagemaker,*,† Frans G. B. Ooms,‡ Erik M. Kelder,‡ Joop Schoonman,‡ Gordon J. Kearley,† and Fokko M. Mulder*,†

Contribution from the Interfaculty Reactor Institute, Delft University of Technology, Mekelweg 15, 2629 JB Delft, and Laboratory for Inorganic Chemistry, Delft University of Technology, Julianalaan 136, 2628 BL Delft, The Netherlands

Received March 24, 2004; E-mail: m.wagemaker@iri.tudelft.nl

Abstract: $Li_xMg_{0.1}Ni_{0.4}Mn_{1.5}O_4$ spinel ($P4_332$) was chemically and electrochemically lithiated in the range $1 < x \leq 2.25$ and subjected to detailed X-ray and neutron diffraction analysis to understand the electrochemical behavior in the 3 V region. Extensive migration of Ni and Mn during lithium insertion was found, resulting in the disappearance of the initial Ni−Mn ordering and the formation of Ni-rich and Ni-poor domains, leading to two Jahn−Teller-distorted tetragonal phases with different Ni:Mn ratios. Such extensive Ni and Mn migration was not known for these spinels, and strongly influences the initial cycling behavior. The newly formed tetragonal phase with a Ni:Mn ratio of ~0.07 has a higher cyclability and a higher capacity, and is therefore suggested to have a favorable composition for this intercalation range, as is confirmed in the literature. In addition, lithium is found to occupy multiple positions inside the distorted oxygen octahedron of this phase, a finding previously known only for lithium in anatase TiO_2.

Introduction

In the past two decades, there has been a vast amount of research devoted to manganese oxide cathode materials for rechargeable Li ion batteries. In comparison with the widely commercialized cobalt oxide, manganese oxide is cheap and less toxic. Although $LiMn_2O_4$ spinel has an attractive theoretical capacity of 148 mAh/g at 4.1 V vs Li/Li^+, the material suffers from capacity loss upon cycling related to the cooperative Jahn−Teller distortion below 3 V vs Li/Li^+ and manganese dissolution.[1,2] Some of the capacity fading observed for spinel manganese oxide can be suppressed by substitution of 5−10% of the Mn atoms with other metal ions. More substantial substitution (25−50%) of Mn by Me = Co, Cr, Cu, Fe, and Ni led to the discovery of the high-voltage spinels $LiMe_{0.5}Mn_{1.5}O_4$ and $LiMeMnO_4$ with potentials between 4.5 and 5 V vs Li/Li^+.[3]

The high-voltage $LiMg_\delta Ni_{0.5-\delta}Mn_{1.5}O_4$ spinels ($0 \leq \delta \leq 0.10$) have been characterized in previous studies.[4,5] Neutron diffraction revealed that the Ni and Mn ions are ordered in the spinel octahedral sites, which reduces the space group symmetry to $P4_332$ ($Fd\bar{3}m$ if Ni and Mn are not ordered)[5] similar to that found for the $LiNi_{0.5}Mn_{1.5}O_4$ spinel.[6] Lithium can be extracted reversibly from $LiMg_\delta Ni_{0.5-\delta}Mn_{1.5}O_4$ ($\delta = 0.05, 0.10$) spinels, and the substitution of Ni + Mg for Mn resulted in better performance and cycling behavior in the high-voltage plateau at 4.7 V vs Li/Li^+.[4] The high voltage of these materials allows the replacement of carbon anodes with materials such as $Li_4Ti_5O_{12}$[7,8] or $LiCrTiO_4$,[9] yet a considerable battery voltage of ~3.2 V is still maintained. These anode materials are thought to be safer and show higher rate capabilities than carbon anodes.

In the present work the electrochemical and structural behavior of $LiMg_{0.1}Ni_{0.4}Mn_{1.5}O_4$ is investigated when extra lithium is inserted into the ordered spinel structure, i.e., $Li_xMg_{0.1}Ni_{0.4}Mn_{1.5}O_4$ with $1 \leq x \leq 2.25$, in the 3 V range (i.e., no extraction in the 4.7 V range). The reports in the literature about lithium insertion into $LiNi_{0.5}Mn_{1.5}O_4$ spinels have shown different electrochemical responses for materials synthesized by low-temperature sol−gel techniques and high-temperature solid-state methods.[10−13] The discharge curves of $LiNi_{0.5}Mn_{1.5}O_4$ vs Li/Li^+ either are flat or show specific steps, an effect which seems to be related to the suppression or formation of a tetragonal second phase, respectively.

† Interfaculty Reactor Institute.
‡ Laboratory for Inorganic Chemistry.

(1) Gummow, R. J.; de Kock, A.; Thackeray, M. M. *Solid State Ionics* **1994**, *69*, 59−67.
(2) Rodriguez-Carvajal, J.; Rousse, G.; Masquelier, C.; Hervieu, M. *Phys. Rev. Lett.* **1998**, *81*, 4660−4663.
(3) Kawai, H.; Nagata, M.; Tukamoto, H.; West, A. R. *J. Power Sources* **1999**, *81*−*82*, 67−72.
(4) Ooms, F. G. B.; Kelder, E. M.; Schoonman, J.; Wagemaker, M.; van Well, A. A.; Mulder, F. M. *Solid State Ionics* **2002**, *152*−*153*, 143−153.
(5) Ooms, F. G. B.; Wagemaker, M.; van Well, A. A.; Mulder, F. M.; Kelder, E. M.; Schoonman, J. *Appl. Phys. A* **2002**, *74*, S1089−S1091.
(6) Gryffroy, D.; Vandenberghe, R. E.; Legrand, E. *Mater. Sci. Forum* **1991**, *79*−*82*, 785.
(7) Zaghib, K.; Simoneau, M.; Armand, M.; Gauthier, M. *J. Power Sources* **1999**, *82*, 300.
(8) Bach, S.; Pereira-Ramos, J. P.; Baffier, N. *J. Power Sources* **1999**, *82*, 273.
(9) Ooms, F. G. B.; Kelder, E. M.; Schoonman, J. *ITE Battery Lett.* **2001**, *2*, B59.
(10) Amine, K.; Tukamoto, H.; Yasuda, H.; Fujita, Y. *J. Electrochem. Soc.* **1996**, *143*, 1607.
(11) Strobel, P.; Ibarra-Palos, A.; Anne, M.; Le Cras, F. *J. Mater. Chem.* **2000**, *10*, 429.
(12) Morales, J.; Sánchez, L.; Tirado, J. L. *J. Solid State Electrochem.* **1998**, *2*, 420−426.
(13) Ariyoshi, K.; Iwakoshi, Y.; Nakayama, N.; Ohzuku, T. *J. Electrochem. Soc.* **2004**, *151*, A296−A303.

10.1021/ja048319x CCC: $27.50

Our interest is to study the changes in the ordered $LiMg_\delta Ni_{0.5-\delta}Mn_{1.5}O_4$ spinels in more detail, in particular the migration of Ni and Mn ions, and to find a relationship between the structural transitions and the electrochemical behavior upon lithium intercalation. It is known that in certain lithium intercalation metal oxides the metal position can be unstable when cycled in a battery. Examples are the migration of Mn ions in layered $LiNi_{1-y}Mn_yO_4$, as the suggested cause for capacity loss,[14] and in Li_xMnO_2, during the layered-to-spinel phase transition,[15] or the migration of Fe in spinel $LiFe_3O_4$ oxides at high temperatures.[16] In these examples, the migration was toward a nonequivalent site, which facilitated the detection of the migration. However, it did not reveal the distance traveled by the metal to its final position. If the metal ion migrated over the sublattice of its original crystallographic position, the migration would be undetectable without tracer experiments.

In the present study, the Ni−Mn ordering in the $Li_1Mg_{0.1}Ni_{0.4}Mn_{1.5}O_4$ spinel provides a unique and sensitive probe for the migration of Ni and Mn, because migration can be expected to disturb the ordering. The experimental sensitivity for the Ni−Mn ordering and for the position of lithium is provided by neutron diffraction, which is applied complementarily to X-ray diffraction. These techniques have a very different sensitivity for Ni and Mn: for X-ray diffraction there is little contrast, while for neutron diffraction there is a very large contrast (Ni, $b_{coh} = 10.3$ fm; Mn, $b_{coh} = -3.73$ fm). A more fundamental understanding of the stability of these spinels, the detailed structural aspects such as metal ion migration, and the relation with the electrochemical performance is of great importance for their application as electrode materials.

Experimental Section

Sample Preparation and Chemical Lithiation. The $LiMg_{0.1}Ni_{0.4}Mn_{1.5}O_4$ spinel was made with a combination of a sol−gel synthesis and solid-state processing.[4] The precursors $LiOH{\cdot}H_2O$ (Merck), $Mg(CH_3COO)_4{\cdot}4H_2O$ (Fluka), $Ni(CH_3COO)_2{\cdot}4H_2O$ (Aldrich), and $Mn(CH_3COO)_2{\cdot}4H_2O$ (Fluka) were ball-milled in distilled water for 15 min. The homogeneous water-based mixture was dried at 110 °C overnight to a homogeneous precursor powder and subsequently calcined in air (three times) at 800 °C for a total of 30 h. The heating and cooling rates for the first two calcination steps were 10 °C/min. The powders obtained in each step were ball-milled in hexane for 30 min using a planetary ball mill with agate jars/balls (Fritsch Pulverisette 7). The final dwell time was 6 h to a slow cooling rate of 0.1 °C/min.

The $Li_xMg_{0.1}Ni_{0.4}Mn_{1.5}O_4$ ($1.25 \le x \le 2.25$) materials were prepared by chemical intercalation with appropriate amounts of *n*-butyllithium in hexane (1.6 M, Aldrich). All sample preparations were carried out in a helium-filled glovebox ($[H_2O] < 5$ ppm). The samples were allowed to react for two weeks at room temperature, after which they were washed twice with clean hexane and dried in the glovebox. In total, five $Li_xMg_{0.1}Ni_{0.4}Mn_{1.5}O_4$ samples were prepared with nominal lithium compositions $x = 1.25$, 1.5, 1.75, 2.0, and 2.25.

Electrochemical Intercalation. For the electrochemical lithiation, $LiMg_{0.1}Ni_{0.4}Mn_{1.5}O_4$ was coated with a doctor blade on 10 μm thick aluminum current collectors using a mixture of carbon black (MMM SuperP), graphite (Timrex SFG10), and poly(vinylidene fluoride) (PVDF; Solvay) dissolved in *N*-methylpyrrolidone (Merck) in a mass ratio of 80:3:10:7. The coatings were dried rapidly under vacuum at 140 °C for ∼10 min followed by drying under vacuum at 80 °C overnight. The resulting coatings were rolled using a Durston roller to densify the coatings and improve the electrical contacts. The final products had a porosity of 40−50% and a smooth, shiny surface and were dried for at least 24 h at 60 °C under vacuum. Samples of Ø = 14−16 mm were cut from the coatings for the electrochemical tests. All electrochemical tests were done in CR2320-type coin cells (Hohsen Corp.). To prevent corrosion of the coin-cell cans (SUS304) at high potentials, the bottoms of the cans were covered with aluminum foil. The cells were assembled in the following stacking order: can, Ø 21 mm × 10 μm Al, cathode sample, Ø 21 mm × 25 μm separator, PP gasket, lithium, spacer plate (Cu, Ø 17 mm × 0.5 mm), Ø 15 mm wave spring, and cap. The electrolyte used was 1 M $LiPF_6$ EC/EMC/DMC (1:2:2 v/v/v) (Mitsubishi Chemical). The PE Solupor separators were obtained from DSM Solutech and were tested previously for their performance.[17] The coin cells were sealed in the helium-filled glovebox. Since the current collectors were not welded to the can, the coin cells were kept under pressure during the tests with a Hoffman clamp to ensure good electrical contact. The electrochemical tests were made with a Maccor S4000 battery tester with the cells controlled at 25.0 ± 0.1 °C in a climate chamber (Vötsch VT4004).

The cells were discharged and charged in steps of 50 μAh using a constant current of *C*/10 (i.e., a 10 h discharge rate based on the active mass and a theoretical capacity of 146.7 mAh/g) followed by a rest period. The open circuit voltage (OCV) was determined after the rest step, which ended when the change in voltage was less than 10 mV/h.

Neutron and X-ray Diffraction. The characterization of the structures of the active materials was made with XRD (Bruker AXS D8 advance, Cu Kα, no filter) and with neutron diffraction. Because subtle changes in structure, lithium positions, and site occupations were expected, both high intensity and high resolution in the *d* spacing are necessary. To meet these demands, the neutron diffraction experiments were performed on the GEM, the high-intensity general-purpose time-off-flight diffractometer at the ISIS pulsed neutron source[18] (Rutherford Appleton Laboratory, U.K.). The instrument is equipped with more than 6000 detectors in 7 banks covering angles between approximately 169° (backscattering) and 6° (forward scattering). All samples were measured at room temperature in cylindrical vanadium airtight sample cans. Data were corrected for the scattering of the vanadium can and the cryostat with the Ariel software.[19] The X-ray and neutron diffraction data were refined simultaneously using the Rietveld method implemented in GSAS.[20] Besides the atomic and lattice parameters, the absorption and line-broadening parameters, the crystal phase fractions, and the background were fitted. To determine the positions of the lithium atoms, Fourier density difference analysis (FDDA) was performed using the difference between observed (intensity due to unknown lithium positions) and calculated (no lithium present) structure factors that were obtained with GSAS. Fourier density difference maps were obtained from the structure factors using the Fourier formalism implemented in the GFour package.[21] The atomic positions suggested from the density difference analysis were subsequently used as input for the Rietveld refinement.

Results

Electrochemical Intercalation. The curves of the first two discharge/charge cycles between 3.5 and 1.0 V for $LiMg_{0.1}Ni_{0.4}Mn_{1.5}O_4$ vs Li/Li^+ are shown in Figure 1. The solid line

(14) Park, H-S.; Hwang, S.-J.; Choy, J-H. *J. Phys. Chem. B* **2001**, *105*, 4860−4866.
(15) Reed, J.; Ceder, G.; van der Ven, A. *Electrochem. Solid State Lett.* **2001**, *4*, A78.
(16) Thackeray, M. M. *J. Am. Ceram. Soc.* **1999**, *82*, 3347−3354.
(17) Ooms, F. G. B.; Kelder, E. M.; Schoonman, J.; Gerrits, J.; Smedinga, N.; Calis, G. *J. Power Sources* **2001**, *97*−*98*, 598.
(18) Williams, W. G.; Ibberson, R. M.; Enderby, P. D. *Physica B* **1998**, *241*−*243*, 234−236.
(19) Radaelli, P. G. http://www.isis.rl.ac.uk/disordered/GEM/Software/Ariel3.1release.htm.
(20) Larson, A. C.; Dreele, R. B. V. *GSAS*; Technical Report NM87545; Los Alamos National Laboratory: Los Alamos, NM, 1994.
(21) Gonzalez-Platas, J.; Rodriguez-Carvajal, J. ftp://charybde.saclay.cea.fr/pub/divers/fullprof.2k/Windows/.

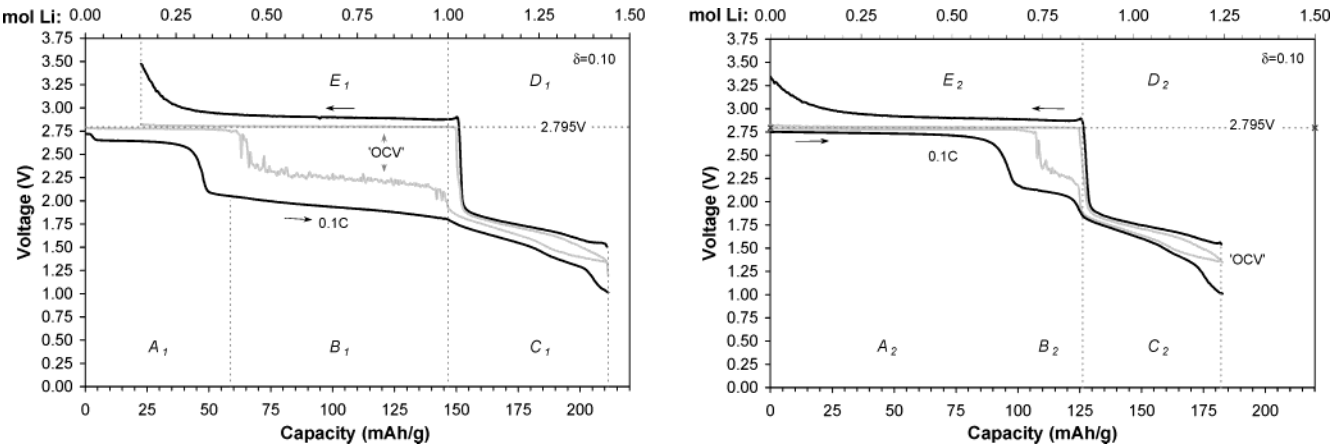

Figure 1. Electrochemical insertion of lithium into $LiMg_{0.1}Ni_{0.4}Mn_{1.5}O_4$ between 3.5 and 1.0 V vs Li/Li^+: constant-current (black) and OCV (gray) curves for the first cycle (left) and the second cycle (right).

represents the *C*/10 rate constant-current curve, and the gray line is the OCV curve. Specific ranges of the curves have been marked with the symbols A_n-E_n for ease of discussion. A subscript $n = 1$ or 2 is added for cycle 1 or 2.

In the first discharge, the insertion of 1 mol of lithium, corresponding to the composition $Li_2Mg_{0.1}Ni_{0.4}Mn_{1.5}O_4$, proceeds in two steps, $A_1 + B_1$, between 3.0 and 1.8 V. Step A_1 is a plateau at 2.7 V, but step B_1 is a sloping curve between 2.1 and 1.8 V. Another 0.44 mol of lithium could be inserted between 1.8 and 1.0 V, step C_1. Subsequent charging shows that the reaction between 1.8 and 1.0 V is reversible, step D_1. Furthermore, the extraction of lithium from $Li_2Mg_{0.1}Ni_{0.4}Mn_{1.5}O_4$ to $LiMg_{0.1}Ni_{0.4}Mn_{1.5}O_4$ proceeds in a single step, E_1, where the flat nature of this plateau indicates a two-phase reaction. The capacity of this two-phase plateau is only 0.85 mol of lithium, which means that active material has been lost. The total loss of capacity in this first cycle is about 23 mAh/g.

The observations from the constant-current curve are supported by the OCV curve, from which it is clear that step A_1 is a two-phase reaction between $LiMg_{0.1}Ni_{0.4}Mn_{1.5}O_4$ and $Li_{1.3}Mg_{0.1}Ni_{0.4}Mn_{1.5}O_4$. Step B_1 has the same slope as in the constant-current curve but at a higher voltage level, indicating a large polarization in this region. Considering the small lithiation steps, leaving the system close to equilibrium, and the OCV criteria of $\Delta V < 0.01$ V/h, it is not expected that the cell voltage in step B will completely relax back to the two-phase voltage of step E_1, although the kinetics is much slower. This means that step B_1 is not simply a two-phase reaction.

The curve of the second cycle shows the same features as found in the first cycle. However, the capacity in the two-phase step A_2 is extended at the expense of step B_2. The capacity in step E_2 ($= A_2 + B_2$) is practically the same as that in step E_1 in the first cycle, ~0.85 mol of lithium. Step C_2 with 0.48 mol is similar to C_1. Thus, in cycle 2 there is almost no capacity loss. It also means that the capacity loss in cycle 1 is related to step A_1 and/or B_1.

Step A_n can be explained with the two-phase conversion of the cubic $LiMg_{0.1}Ni_{0.4}Mn_{1.5}O_4$ phase into a new phase, which is probably a tetragonal phase as has been reported for the system $LiMn_2O_4 \rightarrow Li_2Mn_2O_4$.[22] In step B the conversion of the initial cubic phase continues, but via a different reaction. The end of step B corresponds to the composition $Li_2Mg_{0.1}Ni_{0.4}Mn_{1.5}O_4$. The subsequent two-phase charge reaction E involves only one step, which is likely to be the conversion of tetragonal $Li_2Mg_{0.1}Ni_{0.4}Mn_{1.5}O_4$ into cubic $LiMg_{0.1}Ni_{0.4}Mn_{1.5}O_4$ again. For the ordered $LiNi_{0.5}Mn_{1.5}O_4$ and $LiMg_{0.05}Ni_{0.4}Mn_{1.5}O_{45}$ spinels similar charge/discharge curves for $1 \le x \le 2.25$ were obtained (not shown), indicating that the steps in Figure 1 originate from the ordering in the spinels, and not from the substitution of Mg for Ni.

Chemical Intercalation. Upon lithiation by *n*-butyllithium, a color change was observed for the $Li_xMg_{0.1}Ni_{0.4}Mn_{1.5}O_4$ samples from gray-black via dark brown to light brown. The X-ray diffraction patterns of the samples indicate a conversion of the cubic $P4_332$ phase into a tetragonal phase.

In the neutron diffraction experiments, significant intensities were obtained in the *d* spacing range (0.2−8 Å). In Figure 2, neutron diffraction patterns are shown for two of the five chemically intercalated samples ($x = 1.25$ and 2.25). Figure 2 also contains the neutron diffraction data for a small range in *d* spacing for all samples, including data for the initial spinel $LiMg_{0.1}Ni_{0.4}Mn_{1.5}O_4$ from a previous study.[5] The diffraction patterns clearly reveal the formation of not one but two additional phases upon intercalation (from hereon referred to as T_1 and T_2). In the $Li_{1.25}Mg_{0.1}Ni_{0.4}Mn_{1.5}O_4$ composition the original cubic phase and the first tetragonal phase T_1 coexist, whereas in the $Li_{2.25}Mg_{0.1}Ni_{0.4}Mn_{1.5}O_4$ composition mainly the two tetragonal phases T_1 and T_2 coexist (there is a small fraction of the cubic phase present). Both newly formed phases can be indexed with the tetragonal $I4_1/amd$ space group, but with different unit cell dimensions; see Table 1 and Figure 3. Ex situ X-ray diffraction of the electrochemically intercalated $LiMg_{0.1}Ni_{0.4}Mn_{1.5}O_4$ samples (not shown) confirmed the formation of the two tetragonal phases. However, the data quality of the chemically intercalated samples was much better, which facilitated the following detailed structural analysis.

In general, the Rietveld refinements resulted in residuals Rp and wRp between 3% and 5%. The fractions of the three phases as a function of the overall lithium content in the chemically intercalated samples are shown in Figure 4. The tetragonal phases grow at the expense of the original cubic $P4_332$ phase. The T_1 phase mainly grows in the range $1 \le x \le 1.25$, whereas the T_2 phase mainly grows in the range $1.25 \le x \le 2.25$. This suggests the existence of two different regions of phase equilibrium, which is confirmed by the electrochemical data in

(22) Ohzuku, T.; Kitagawa, M.; Hirai, T. *J. Electrochem. Soc.* **1990**, *137*, 769.

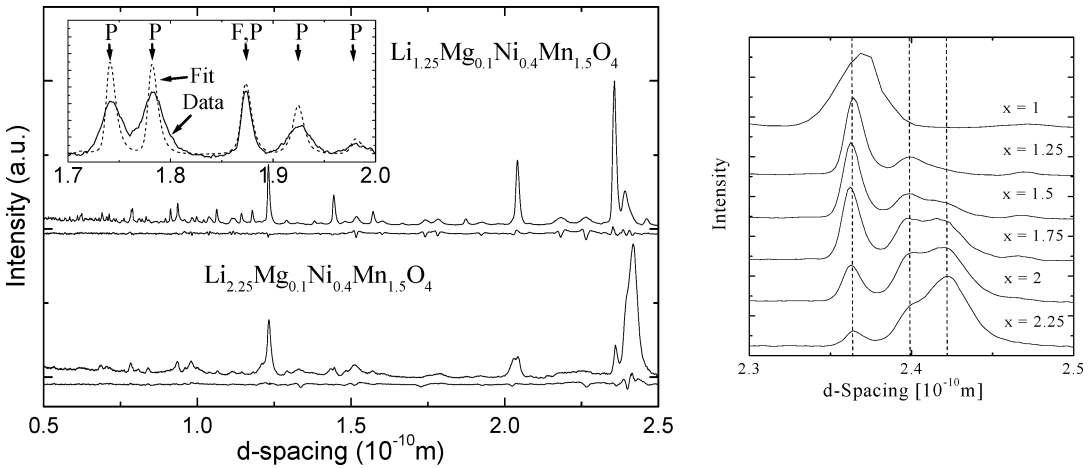

Figure 2. Left: neutron diffraction patterns for two compositions, including the difference between the fitted and the observed intensities. The inset illustrates the different line widths of the reflections originating from the ordered and nonordered spinels, respectively, indicated by "*P*" ($P4_332$) and "*F*" ($Fd\bar{3}m$). Right: small range of the neutron diffraction patterns for all $Li_xMg_{0.1}Ni_{0.4}Mn_{1.5}O_4$ samples including the pattern for $LiMg_{0.1}Ni_{0.4}Mn_{1.5}O_4$ from a previous study.[5]

Table 1. Atom Positions of the Three Phases in Lithiated $Li_xMg_{0.1}Ni_{0.4}Mn_{1.5}O_4$ from Simultaneous Rietveld Refinements of Neutron and X-ray Diffraction Data[a]

phase	atom	site	*x*/*a*, *y*/*b*, *z*/*c*	fraction [0–1]
Refined from a Sample with Composition $Li_{1.25}Mg_{0.1}Ni_{0.4}Mn_{1.5}O_4$				
$P4_332$ (212),	Li	8c	−0.001	0.81
$a = 8.1571$ Å	Li	4a	1/8	0.35
	Mg	4b	5/8	0.20
	Ni	4b	5/8	0.57
	Mn	4b	5/8	0.23
	Ni	12d	1/8, 0.378, 0.872	0.05
	Mn	12d	1/8, 0.382, 0.868	0.95
	O	8c	0.387	1.00
	O	24e	0.104, 0.126, 0.393	1.00
Refined from a Sample with Composition $Li_{2.25}Mg_{0.1}Ni_{0.4}Mn_{1.5}O_4$				
$I4_1/amd$ (T_1) (141),	Li	4a (8c)	0, 3/4, 1/8	0.40
$a, b = 5.7375$ Å,	Li	16h	0, 0.0235, 0.0558	0.50
$c = 8.6575$ Å	Mg	8d (12d/4b)	0, 0, 1/2	0.05
	Ni	8d (12d/4b)	0, 0, 1/2	0.06
	Mn	8d (12d/4b)	0, 0, 1/2	0.89
	O	16h (8c/24e)	0, 0.485, 0.732	1.00
$I4_1/amd$ (T_2) (141),	Li	8c (12d/4a)	0	0.90
$a, b = 5.7175$ Å,	Ni	4a (8c)	0, 3/4, 1/8	0.07
$c = 8.9936$ Å	Mg	8d (12d/4b)	0, 0, 1/2	0.05
	Ni	8d (12d/4b)	0, 0, 1/2	0.24
	Mn	8d (12d/4b)	0, 0, 1/2	0.68
	O	16h (8c/24e)	0, 0.487, 0.735	1.00

[a] The results for the cubic phase are from the sample with composition $Li_{1.25}Mg_{0.1}Ni_{0.4}Mn_{1.5}O_4$, and for the tetragonal phases from the sample with composition $Li_{2.25}Mg_{0.1}Ni_{0.4}Mn_{1.5}O_4$. The coordinates for the $I4_1/amd$ space group are given in origin choice 2. The space group number is noted in parentheses. If only one coordinate is given, it implies $x = y = z$ for that atom. The Wyckof site notations in $I4_1/amd$ are followed by the equivalent positions in $P4_332$. Space groups $P4_332$ and $I4_1/amd$ contain, respectively, eight and four formula units of $LiMg_{0.1}Ni_{0.4}Mn_{1.5}O_4$.

Figure 1, steps A and B. A comparison of the unit cell dimensions shows that a large lattice deformation occurs when the initial cubic phase ($P4_332$) is converted into the tetragonal phases, as illustrated in Figure 3. The lattice shrinks in the $a_T = b_T$ directions, amounting to 0.63% for the T_1 phase and 0.97% for the T_2 phase (the tetragonal unit cell dimensions $a_T = b_T$ compare to $\sqrt{2}a_C$ of the cubic unit cell). However, there is a large expansion in the *c*-directions, 6.1% for the T_1 phase and 10.1% for the T_2 phase.

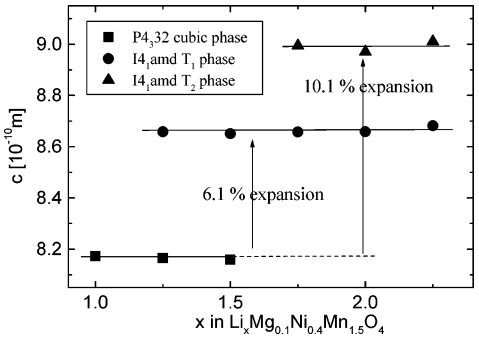

Figure 3. Lattice expansion of the *c* axis of the two tetragonal phases relative to the original cubic phase as a function of the lithium content. The size of the symbols represents the size of the error bars.

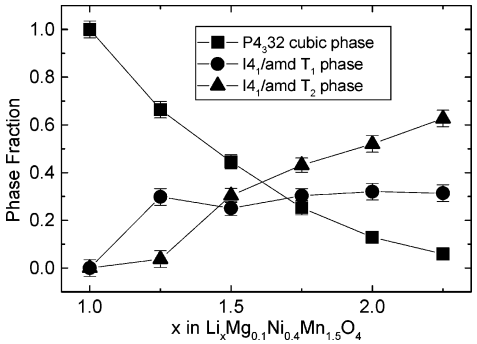

Figure 4. Phase fractions from Rietveld refinement as a function of the overall lithium content in the chemically lithiated $LiMg_{0.1}Ni_{0.4}Mn_{1.5}O_4$ samples.

Ni−Mn Ordering. Due to the random occupation of the octahedral positions by Mn and Ni, the neutron diffraction patterns had to be indexed with the $I4_1/amd$ space group (No. 141). If the Ni−Mn ordering, which is present in the initial cubic phase ($P4_332$), persisted during the phase transition, then the diffraction patterns should allow indexing with the ordered $P4_32_12$ space group (No. 96), which has distinct differences in neutron diffraction line intensities compared to the nonordered $I4_1/amd$ structure. Therefore, the conclusion is that the Ni−Mn ordering is lost upon lithium intercalation of the ordered $P4_332$ spinel. Note that this would not have been detected with X-ray

diffraction as a result of the small difference in scattering length for X-rays between Mn and Ni.

Length Scale of the Ni−Mn Ordering. The reflections originating from both tetragonal phases display considerable line broadening compared to the instrumental resolution, which will be discussed later. First, we will discuss the line broadening effects of the cubic phase. The neutron diffraction pattern of the sample with composition $Li_{1.25}Mg_{0.1}Ni_{0.4}Mn_{1.5}O_4$ in Figure 2 shows an interesting phenomenon related to the Ni−Mn ordering. Close observation of the reflections that originate from the initial cubic $P4_332$ phase reveals that some of them are much broader than others; see the inset in Figure 2. To explain this, we note that the Ni−Mn ordering reduces the normal spinel symmetry from cubic $Fd\bar{3}m$ to the present cubic $P4_332$ space group,[5] resulting in extra reflections (indicated by "*F*" and "*P*", respectively, in the inset in Figure 2). Only the additional *P* reflections that arise due to the symmetry reduction are broadened. This selective broadening phenomenon was not observed before because the line width of the previous neutron diffraction pattern[5] for $x = 1.0$ in Figure 2 was of insufficient resolution to resolve the line broadening.

The main differences between the fitted and observed intensities in Figure 2 are due to these broad ($P4_332$) reflections, as can be seen by close observation of the difference curve. These broadened reflections can be associated with the Ni−Mn ordering, which leads to the interpretation that the length scale of the Ni−Mn ordering is small compared to the size of the crystallites. Apparently, the Ni−Mn ordering does not proceed through a whole crystallite, but instead a crystallite consists of ordered domains. In the initial cubic phase, all the Ni and Mn ions are ordered, albeit in domains of limited length scale, because the cubic phase could not be fitted by a sum of an ordered phase and a nonordered phase. The fitted line width of these reflections gives an idea of the size of the Ni−Mn domains. The result is approximately 13 nm, whereas the size of the crystallites is 0.5−1 μm,[4] consistent with the narrow X-ray diffraction lines. The ordering, and thus the length scale of the domains, is thought to be the result of the synthesis procedure, in particular of the slow cooling step in the annealing process.

Domain Size and Strain in the Tetragonal Phases. The initial cubic phase leads to reflections narrower than the instrumental resolution, except for the reflections that are related to the limited extent of the Mn−Ni ordering, as described in the previous paragraph. The considerable line broadening of the two tetragonal phases, which occurs upon lithiation, could be the result of reduced particle sizes and/or internal stress, but it is difficult to distinguish between these two effects. Assuming it to be the result from particle size broadening, an approximate value of the particle sizes can be obtained from the line widths. This results in particles of ~40 nm for the T_1 phase and ~10 nm for the T_2 phase.

Atomic Positions and Fractions in the Cubic and Tetragonal Phases. Rietveld refinement also resulted in detailed information of the atom fractions and positions in the three phases, as listed in Table 1. A significant difference in the Ni:Mn ratio of the two tetragonal phases is observed; see Figure 5. The Ni:Mn ratio of the three phases was allowed to vary independently during the refinement, but the total Ni:Mn ratio in the system was kept constant at 0.2667, corresponding to the ratio in $LiMg_{0.1}Ni_{0.4}Mn_{1.5}O_4$. The small fraction of Mg in the system, which is also located in the octahedral 8d sites, was kept constant. This means that the Mg migration toward other positions was not considered, mainly because the Ni:Mn ratio effects dominate in this system. The Ni:Mn ratio in the T_1 phase clearly varies as function of lithium content between 0.18 ($x = 1.25$) and 0.07 ($x = 2.25$), but it is rather constant around 0.44 in the T_2 phase. Apparently, the formation of the T_2 phase is favorable, with the T_1 phase donating the amount of Ni required by the T_2 phase in which Ni substitutes for Mn. In this way, Ni-rich clusters form the basis for the formation of the T_2 phase, whereas Mn-rich clusters form the basis for the T_1 phase. The variation of the Ni:Mn ratio between the two tetragonal phases probably causes the difference in lattice expansion (Table 1).

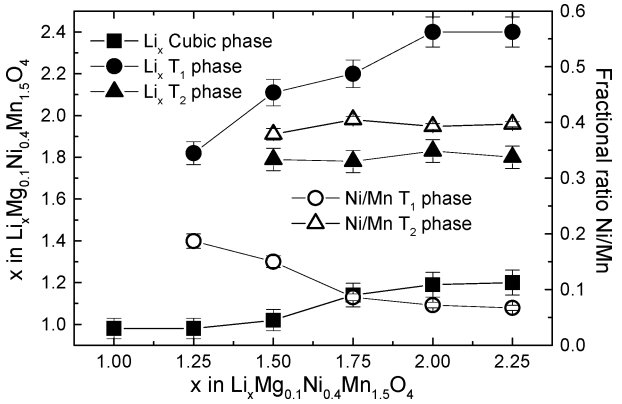

Figure 5. Lithium content x in the cubic, T_1, and T_2 phases and the Ni:Mn ratios.

The notion that Mn and Ni can move within the lattice motivated the search for other lattice positions for Ni and Mn. In the T_2 phase, a small Ni fraction appears to reside on the tetrahedral 4a position; see Table 1. In the T_1 phase, the 4a sites are (not fully) occupied with Li only (which has a negative scattering length, $b_{coh} = -1.9$), but in the T_2 phase the 4a sites appear to be filled by atoms with a positive scattering length for neutrons. Assuming that oxygen remains on its site, the only atoms in this material having a positive scattering length are Mg ($b_{coh} = +5.37$ fm) and Ni ($b_{coh} = +10.3$ fm). Further refinement leads to the conclusion that at least a small Ni fraction (5−10%, depending on the overall Li contents) is located on the 4a position together with Li. However, a combination of Ni and Li, and/or Mg, cannot be excluded.

Lithium Positions. The relative sensitivity of neutrons for lithium allows the accurate determination of their positions in the spinel host structure. In principle, Li positions with occupation fractions as low as 1% can be found by a Fourier density difference analysis (FDDA) of the diffraction pattern.[23] To illustrate the difference in lithium occupation between the three phases, the equivalent positions of the tetragonal phases in the cubic space group are given in Table 1. FDDA indicated that in the T_1 phase lithium does not simply occupy the center of an oxygen octahedron, i.e., the 8c position in $I4_1/amd$ (12d/4a in $P4_332$ and 16c in $Fd\bar{3}m$). Instead, lithium can occupy one of two discrete positions within an oxygen octahedron, i.e., the 16h sites in the $I4_1/amd$ space group; see Figure 6. Further refinement with these new lithium positions resulted in a significant improvement of the fit quality and the correct lithium

(23) Wagemaker, M.; Kearley, G. J.; van Well, A. A.; Mutka, H.; Mulder, F. M. *J. Am. Chem. Soc.* **2003**, *125*, 840−848.

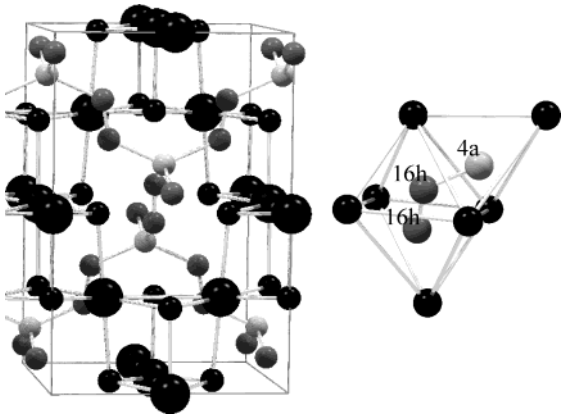

Figure 6. Left: unit cell of the T_1 phase (space group $I4_1/amd$) (small black spheres, oxygen atoms; large black spheres, Mn, Ni, and Mg positions; small dark-gray spheres, Li 16h positions; small light-gray spheres, Li 4a positions). Right: isolated oxygen octahedron and tetrahedron including the Li 16h−16h−4a path.

content, thereby confirming and quantifying these split octahedral lithium positions (see Table 1). Although a similar 8c position splitting could be expected for the T_2 phase, refinement did not result in an unambiguous preference for lithium to reside on the 16h positions. We anticipate that this is due to the increased disorder in this phase, characterized by the broad diffraction reflections, which prevents a more detailed refinement. Therefore, lithium was refined in the center of the oxygen octahedron for the T_2 phase (8c position).

The lithium fractions in the cubic and T_1 phases increase during lithium intercalation, whereas the lithium fraction in the T_2 phase is rather constant around 1.8, as illustrated in Figure 5. A comparison of the lithium phase fractions for the fully lithiated sample $Li_{2.25}Mg_{0.1}Ni_{0.4}Mn_{1.5}O_4$ shows that most of the additional lithium is found in the T_1 phase. The atom fractions for this sample lead to the following phase compositions: cubic, $Li_{1.2}Mg_{0.1}Ni_{0.4}Mn_{1.5}O_4$ (not in Table 1); T_1, $Li_{2.4}Mg_{0.1}Ni_{0.12}Mn_{1.78}O_4$; T_2, $Li_{1.8}Mg_{0.1}Ni_{0.54}Mn_{1.36}O_4$.

Discussion

Phase Transitions. A remarkable observation in the present study is that, by chemical lithiation of $Li_xMg_{0.1}Ni_{0.4}Mn_{1.5}O_4$ in the range $1.0 \le x \le 2.25$, the initially cubic Ni−Mn ordered spinel is gradually converted into two tetragonal phases, instead of one, both indexed with the $I4_1/amd$ space group. The tetragonal phases differ significantly in their lattice parameters and chemical compositions. The T_1 phase contains a larger amount of lithium and has a lower Ni:Mn ratio than the T_2 phase. The Ni:Mn ratio in the T_2 phase is constant as a function of the overall lithium content, whereas the T_1 phase hosts the remaining Ni and Mn. As noted before, the large contrast between Ni and Mn facilitates the accurate determination of site occupations. The composition of both phases can be used to calculate the average valence of manganese, n_{Mn}, in the cubic and tetragonal phases, assuming a divalent state for Ni and Mg. In the initial material (i.e., $LiMg_{0.1}Ni_{0.4}Mn_{1.5}O_4$ from a sample with $x = 1.25$) this leads to $n_{Mn} = 4$, in the T_1 phase (i.e., $Li_{2.4}Mg_{0.1}Ni_{0.12}Mn_{1.78}O_4$ from a sample with $x = 2.25$) to $n_{Mn} = 2.90$, and in the T_2 phase (i.e., $Li_{1.8}Mg_{0.1}Ni_{0.54}Mn_{1.36}O_4$ from a sample with $x = 2.25$) to $n_{Mn} = 3.92$. This simple consideration suggests that manganese predominantly exists as Mn^{3+} in the T_1 phase and as Mn^{4+} in the T_2 phase.

At first, the larger lattice expansion of the T_2 phase compared to the T_1 phase might be explained by the higher fraction of Ni in the T_2 phase combined with the larger ionic radius of Ni^{2+} (0.70 Å)[24] compared to Mn^{4+} (0.54 Å). However, this would probably lead to an isotropically larger unit cell. In contrast to that, T_2 shrinks along the *a* and *b* lattice directions and expands along *c*, see Table 1, which suggests a stronger Jahn−Teller distortion compared to that of the T_1 phase. An explanation could be the presence of Jahn−Teller-active Ni^{3+}, which imposes a higher fraction of Jahn−Teller-active Mn^{3+}. But without knowledge of the valence states of Ni and Mn, a definitive explanation cannot be given.

Initially, a lithium content of 2.4 in the T_1 phase seems too high when only the octahedral 8c sites are considered, which would limit the number of lithium sites to 2 (1 tetragonal unit cell contains 4 formula units of $LiMg_{0.1}Ni_{0.4}Mn_{1.5}O_4$). However, if lithium is allowed to coexist in the tetrahedral 4a sites, then there are 3 lithium sites per $LiMg_{0.1}Ni_{0.4}Mn_{1.5}O_4$ unit. Effectively, the amount of reducible Mn^{4+} limits this electronically to 2.5, resulting in $Li_{2.5}Mg_{0.1}Ni_{0.4}Mn_{1.5}O_4$. Table 1 shows that lithium was indeed found on 8c as well as 4a sites. This reasoning was also used by Ariyoshi et al. to explain the existence of step C (1.8−1.0 V) in the discharge curves, where they still detected a tetragonal phase.

A cubic to tetragonal phase transition is known for other manganese spinels such as $LiMn_2O_4$, $Li_2Mn_4O_9$, and $Li_4Mn_5O_{12}$. The reason for this transition is a cooperative Jahn−Teller distortion of the $Mn^{3+}O_6$ octahedra when the fraction of Mn^{3+} ($t_{2g}^3e_g^1$) Jahn−Teller ions becomes more than 0.5 or, equivalently, if the average manganese valence n_{Mn} drops below 3.5. For $LiMn_2O_4$, $n_{Mn} = 3.5$ and the insertion of extra lithium (i.e., the reduction of Mn^{4+} to Mn^{3+}) immediately results in the formation of a tetragonal phase. However, in $Li_2Mn_4O_9$ and $Li_4Mn_5O_{12}$, $n_{Mn} = 4.0$, and their lattices were reported to remain cubic upon insertion of ~2 mol of lithium per formula unit (i.e., close to $n_{Mn} < 3.5$) before a tetragonal phase was formed.[25] Thus, on the basis of the critical Mn^{3+} concentration alone, it was expected that in $LiMg_{0.1}Ni_{0.4}Mn_{1.5}O_4$ or $LiNi_{0.5}Mn_{1.5}O_4$ with $n_{Mn} = 4.0$ a cubic to tetragonal phase transition would not take place before the insertion of 0.75 mol of lithium, but the literature shows different results.

For $Li_xNi_{0.5}Mn_{1.5}O_4$ ($1 \le x \le 2$) produced with sol−gel synthesis, Amine et al.[10] observed only a small increase in the cubic lattice parameter from 8.1744 Å at $x = 1$ and 8.1764 Å at $x = 2$, but not the formation of a tetragonal phase. This was confirmed by the electrochemical lithiation of nonordered $LiNi_{0.5}Mn_{1.5}O_4$ ($Fd\bar{3}m$) by Strobel et al.,[11] although they did find one tetragonal phase using chemical lithiation. Later, they also reported the ordering of Ni and Mn for $LiNi_{0.5}Mn_{1.5}O_4$ ($P4_332$), but no lithiation experiments.[26] Recently, Ariyoshi et al.[13] reported the appearance of one tetragonal phase upon lithiation of solid-state-synthesized ordered $Li_xNi_{0.5}Mn_{1.5}O_4$ ($P4_332$) with lattice parameters that are in good agreement with those of the T_1 phase here. Both groups used X-ray diffraction only for the structural characterizations.

(24) Shannon, R. D. Revised effective ionic radii in halides and chalcogenides. *Acta Crystallogr.* **1976**, *A32*, 751.
(25) Thackeray, M. M.; de Kock, A.; Rossouw, M. H.; Liles, D.; Bittihn, R.; Hoge, D. *J. Electrochem. Soc.* **1992**, *139*, 363−365.
(26) Strobel, P.; Ibarra-Palos, A.; Anne, M.; Poinsignon, C. A. *Crisci Solid State Sci.* **2003**, *5*, 1009−1018.

Interestingly, the discharge curves of $LiNi_{0.5}Mn_{1.5}O_4$ reported by Ariyoshi et al. display two very similar steps as reported here for the $Li_xMg_\delta Ni_{0.5-\delta}Mn_{1.5}O_4$ materials. In the work of Strobel et al. only the onset of this second step can be seen because of the higher cutoff voltage used (2.3 V). In the present study, the second plateau (step B in Figure 1) is suggested to be the result of the second tetragonal phase T_2, and because of the similarities in the discharge curves, we expect that the T_2 phase is also present in the materials reported by Ariyoshi et al. and Strobel et al. A possible explanation of why the T_2 phase was not detected by Strobel et al. and Ariyoshi et al. is that the T_2 phase is more difficult to detect with X-ray diffraction than the T_1 phase due to substantial line broadening. Even in this study, the use of X-ray diffraction alone would have revealed neither the T_2 phase nor the Ni-rich and Mn-poor domains, which were found by neutron diffraction.

All the materials which were reported to have no cubic to tetragonal transition ($Li_2Mn_4O_9$, $Li_4Mn_5O_{12}$,[25] and $LiNi_{0.5}Mn_{1.5}O_4$[10]) were made by low-temperature sol−gel techniques (~400 °C). In general, this technique leads to small particles with a low degree of crystallinity, in contrast to materials synthesized by high-temperature solid-state techniques (750−900 °C), resulting in high crystallinity, even cationic ordering, and well-defined particles (sometimes small single crystals). It seems that $LiNi_{0.5}Mn_{1.5}O_4$ and $LiMg_\delta Ni_{0.5-\delta}Mn_{1.5}O_4$ materials with high crystallinity (and possibly ordering) show a cubic to tetragonal transition as well as a second step in the discharge curve while sol−gel materials do not. Consequently, the cyclability of these manganese oxides, when used as insertion electrode materials, is much better when derived from sol−gel than from solid-state synthesis. Morales et al. demonstrated this loss of cyclability for Ni-substituted $LiMn_2O_4$ synthesized at different temperatures.[12] An explanation for this loss[11,12] is that very small, disordered particles are able to cope with the local Jahn−Teller effects by elastic deformation while highly crystalline particles fracture under the long-range cooperative distortion.

Ni−Mn Ordering and Migration. The disappearance of the Ni−Mn ordering due to the phase transition from cubic to tetragonal implies that Ni and Mn migrate over the 12d/4b positions (in $P4_332$), thereby destroying the ordering. Moreover, it was found that the two tetragonal phases differ significantly in the Ni:Mn ratio, whereas these ions were evenly distributed over the initial cubic crystal. This variation of the Ni:Mn ratio is another indication that Ni and Mn migrate during the Li insertion. The particle size broadening of the two tetragonal phases (to 40 and 10 nm) illustrates the length scale over which the migration extends. It is reasonable to suggest that the Ni and Mn migration takes place over a length scale on the order of the Ni−Mn ordering domain size, i.e., ~13 nm. These distances are comparable with those of the initial Ni−Mn ordering. Therefore, we conclude that the migration of Ni and Mn destroys the ordering and is also responsible for the formation of new domains that differ in Ni:Mn ratio.

For layered $LiMnO_2$ Park et al. found that, during lithium extraction and insertion, Mn ions migrate to interlayer positions, leading to a structural modification that is responsible for the capacity loss when used in a battery.[14] This appears to be a more general issue in layered oxide materials. The results of Park et al. can be understood by metal ion migration toward a neighboring site, which is a very limited distance of ~2 nm. In contrast to that, the results obtained in this study imply that Ni and Mn migrate over distances on the order of ~10 nm. To our knowledge, such an extensive migration and rearrangement of metal ions in a lithium intercalation electrode material has not been reported before, and opens a new aspect to be taken into account when the stability of these materials during (dis)charge is studied. It suggests that in some transition-metal oxides the energy barrier for the metal ion can become sufficiently low during lithium intercalation to allow extensive migration, even at room temperature, which is supported by the low activation energy, 0.2 eV, as calculated by Reed et al. for Mn in Li_xMnO_2.[15] The Ni migration in the T_2 phase leads to a Ni fraction of 0.07 on the 4a positions, which in the T_1 phase are occupied by Li. We were unable to find literature reporting on extensive Ni or Mn migration in spinel materials toward Li positions; however, for Fe it has been reported for lithium intercalation in spinel Fe_3O_4.[16] In spinel Fe_3O_4, a fraction of the Fe ions move toward the 16c positions and a fraction of Fe is replaced by lithium, resulting in the extrusion of elemental Fe. Explicit Fe migration distances were not reported. The Fe ions on the 16c sites hinder the Li ion diffusion and make the reaction irreversible. Similarly, we expect that the Ni ions on the Li positions will hinder the diffusion of lithium in the T_2 phase.

Detailed Li Ion Positions. The occurrence of two lithium positions within the oxygen octahedra can be understood if the structural transition from the cubic to the tetragonal phases is considered. The Jahn−Teller distortion of the MnO_6 octahedra invokes a lattice expansion and thus a stretching of all the MO_6 octahedra in the *c* direction. As a result, the single central LiO_6 position is split into two positions located above and below the four equatorial oxygen atoms (i.e., in the $+c$ and $-c$ directions), thereby lowering the strong van der Waals repulsive interaction in the *ab* plane. In the $I4_1/amd$ space group this leads to a change of the site symmetry and multiplicity from 8c to 16h. Because the distance between two 16h positions is only ~1 Å, both positions cannot be occupied simultaneously. The lithium positions in the newly formed T_1 phase are indicated in Figure 6, including the two discrete 16h positions within the oxygen octahedron and the 4a tetrahedral positions. Close inspection of Figure 6 reveals that the two 16h positions are not precisely aligned with the *c* direction, but are positioned toward the face-sharing 4a positions (8c in $P4_332$) with a 16h−4a distance of only ~1.5 Å. Therefore, the most probable diffusion path for the Li ions is easily recognized as 16h−16h−4a−16h−16h−4a (or the equivalent path in the $Fd\bar{3}m$ space group is 16c−8a−16c−8a). For the spinel $Li[Mn_{1.96}Li_{0.04}]O_4$ it was demonstrated that Li ions indeed diffuse through the material by occupying both the tetrahedral and octahedral sites[27].

The notion of multiple Li ion sites in deformed oxygen octahedra is relatively new and was first reported in lithiated anatase TiO_2.[23] Such multiple Li positions can only be detected with high-resolution neutron diffraction collected over a large range of *d* spacings, such as provided by the GEM[18] at ISIS (U.K.). This second occurrence of split sites in a deformed oxygen environment suggests it to be a more general effect.

(27) Verhoeven, V. W. J.; de Schepper, I. M.; Nachtegaal, G.; Kentgens, A. P. M.; Schoonman, J.; Mulder, F. M. *Phys. Rev. Lett.* **2001**, *86*, 4314.

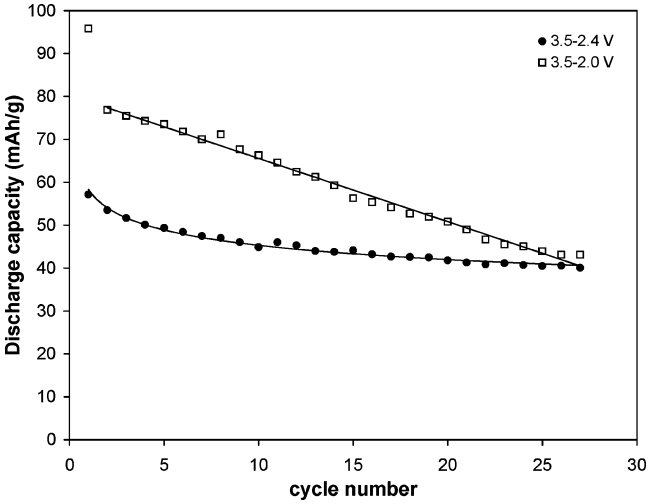

Figure 7. Cyclability of $LiMg_{0.1}Ni_{0.4}Mn_{1.5}O_4$ vs Li/Li^+ with different lower cutoff voltages at a 0.1*C* rate (solid circles, 3.5−2.4 V; open squares, 3.5−2.0 V).

Relation of Structure with Electrochemistry. On the basis of the detailed structural information of the chemically lithiated samples, the following lithium insertion scheme is proposed to explain the charge/discharge curves as shown in Figure 1. The appearance of the T_1 phase in the range $x = 1-1.25$ (Figure 4) suggests that the first potential plateau at about 2.7 V vs Li/Li^+ is related to the coexistence of the initial cubic phase with this T_1 phase. During the intercalation of lithium and the phase transition, the migration of the Mn and Ni ions destroys the initial Ni−Mn ordering. Further intercalation of lithium results in the formation of the T_2 phase (Figure 4), which has a relatively high Ni:Mn ratio compared to the initial phase. The formation of the Ni-rich T_2 phase is consistently accompanied by a decrease in the amount of Ni in the T_1 phase. Although intercalation in the range $x = 1.25-2.25$ predominantly results in the formation of the T_2 phase (the T_1 phase fraction grows only marginally), the T_1 phase progressively takes up more lithium, as is illustrated in Figure 5. Therefore, step B at about 2 V vs Li/Li^+ is not only associated with the formation of the T_2 phase, but also reflects a mixed potential of lithium in both tetragonal phases. The fact that this plateau is not flat is ascribed to the variation of the lithium concentration in the T_1 phase and the migration of Ni and Mn, which changes the Ni:Mn ratio in the T_1 phase due to the formation of the Ni-rich T_2 phase. The decrease of the average Ni:Mn ratio in the T_1 phase, which means an increase of reducible Mn^{4+}, results in the accommodation of additional lithium in the T_1 phase.

At the beginning of the second cycle, the tetragonal phases are converted back into a cubic phase, with the difference that Ni-rich and Ni-poor domains have been formed in the first cycle. Subsequent lithium insertion again leads to the formation of the T_1 phase, although this time not hindered by the formation of the Ni-rich and Ni-poor domains, because they are already present. The increased intercalation capacity of the T_1 phase, due to the smaller Ni:Mn ratio, can now be fully utilized from the start of the second cycle. On the basis of the fraction of the T_1 phase at composition $x = 2.25$ (31%; see Figure 4), and the amount of lithium that can be inserted into it at the end of the first cycle (2.4 mol; see Figure 5), the capacity of the T_1 phase in the second cycle evaluates to 0.74 mol of lithium, which is close to the observed 0.65 mol of the first plateau in the second cycle; see Figure 1. This shows that in the second cycle most of the capacity of the T_1 phase is utilized before the T_2 phase is formed and that the first plateau has a larger capacity in the second cycle compared to the first cycle (0.35 mol of lithium).

The second intercalation step, B_2, mainly associated with the formation of the T_2 phase, has a lower capacity compared to step B_1 for three reasons: (1) Due to the higher Ni:Mn ratio, step B_2 starts with a material having less Mn^{4+} that can be reduced. (2) The large anisotropic increase of the unit cell of the T_2 phase (Figure 3) will result in considerable capacity fading. (3) The Ni fraction that migrated to the tetrahedral 4a lithium positions will hinder the diffusion of lithium through the T_2 phase. Unfortunately, the changes in composition due to the Ni and Mn migration result in the formation of the T_2 phase, and also lead to the T_1 phase with a Ni:Mn ratio of ∼0.07, which shows a reasonable cyclability. This is illustrated in Figure 7 by comparing the cyclability between 3.5−2.4 and 3.5−2.0 V with a 0.1*C* rate. The capacities obtained in both regimes are rather low, but where the capacity fading is almost linear in the 3.5−2.0 V regime, it quickly stabilizes in the 3.5−2.4 V regime. This suggests that a material synthesized with a Ni:Mn ratio of 0.07 ($LiMg_{0.1}Ni_{0.13}Mn_{1.87}O_4$) instead of 0.2667 ($LiMg_{0.1}Ni_{0.4}Mn_{1.5}O_4$) will perform better, especially if small particles are synthesized. This suggestion is supported by the study of Morales et al.,[12] who reported enhanced cycling behavior for lithium insertion in $Li_xNi_{0.15}Mn_{1.85}O_4$ compared to $Li_xMn_2O_4$ ($1 \le x \le 2$), a composition very close to $LiMg_{0.1}Ni_{0.13}Mn_{1.87}O_4$ suggested here.

Concluding Remarks

Detailed structural data were obtained for $Li_xMg_{0.1}Ni_{0.4}Mn_{1.5}O_4$ spinels, intercalated with lithium in the range $1 \le x \le 2.25$, by simultaneous Rietveld refinement of X-ray and neutron diffraction data. On the basis of the structural information, the electrochemical cycle behavior has been explained. One of the most important observations in this study is the extensive migration of Ni and Mn, resulting in Ni-rich and Ni-poor domains. In particular, the disappearance of the initial Ni−Mn ordering in these materials, which appears to exist over a length scale of approximately 13 nm, clearly illustrates Ni and Mn migration during Li intercalation. The low Mn concentration and the large lattice deformation of the Ni-rich domains, in combination with the hindering of the lithium diffusion in these domains, are responsible for the capacity fading of these materials. However, the Ni-poor domains form a phase that has a reasonable cycling behavior and a high Li capacity, suggesting the use of this composition as starting material. Detailed analysis of the Li ion positions revealed that Li occupies multiple positions inside a distorted oxygen octahedron, a second example in the literature.

Acknowledgment. This work is a contribution from the Delft Institute for Sustainable Energy (DISE). Financial support from the Netherlands Organization for Scientific Research (NWO) is gratefully acknowledged. We thank Laurent Chapon for assistance with the diffraction measurements.

Supporting Information Available: A table of coordinates for the minimized $Li_xMg_{0.1}Ni_{0.4}Mn_{1.5}O_4$ compositions (CIF). This material is available free of charge via the Internet at http://pubs.acs.org.

JA048319X